Symmetries in Bayesian Extended Object Tracking

FLORIAN FAION
ANTONIO ZEA
MARCUS BAUM
UWE D. HANEBECK

In this work, we exploit geometric symmetries in extended objects in order to improve Bayesian tracking algorithms that use Spatial Distribution Models, Greedy Association Models as used in curve fitting, and Random Hypersurface Models. The key idea is to describe symmetric objects by solely modeling the non-redundant part of the shape, while the remainder of the shape follows from symmetry. Following this idea, we develop simplified versions for the three models that take advantage of the symmetry. Exploiting symmetries yields two major benefits. First, complex symmetric shapes can be equivalently represented by a fraction of the original shape parameters. Second, when using sample-based filters, such as the widely used Unscented Kalman Filter, symmetry yields a higher effective sample resolution. It is worth mentioning that estimating even simple objects such as a stick, which only have one reflectional symmetry, can be significantly improved.

Manuscript received November 22, 2013; revised June 14, 2014; released for publication September 13, 2014.

Refereeing of this contribution was handled by Peter Willett.

Authors' addresses: F. Faion, A. Zea, and U. Hanebeck, Intelligent Sensor-Actuator-Systems Laboratory (ISAS), Institute for Anthropomatics and Robotics, Karlsruhe Institute of Technology (KIT), Germany (e-mail: florian.faion@kit.edu, antonio.zea@kit.edu, uwe.hanebeck@ieee.org). M. Baum, University of Connecticut, USA, (e-mail: baum@engineer.uconn.edu).

1 INTRODUCTION

Tracking shape and pose of extended objects based on point measurements is a well-studied task that spans many different fields of research including robotics, human machine interaction, and surveillance. In the context of tracking, the difference between a classical object and an extended object is that the former is, due to its size or sensor resolution, assumed to produce measurements from one distinct source on the shape, while the latter is assumed to produce measurements from more than one source. Depending on the specific task, there are different sensors available to capture point measurements of a given target object. These include laser scanners, depth cameras, and radars, all of which produce data that differ in both the quantity and the quality (i.e. uncertainty) of the measured points. In addition to these sensor-specific characteristics, (self-)occlusions and unknown association of measured points to its generating sources on the object are the main challenges when tracking an extended object.

Many objects in everyday life have known geometric symmetries and incorporating them into tracking algorithms makes sense for two reasons. First, it allows for modeling only a small part of the shape, and then using symmetry to obtain the other parts, which can be exploited to reduce the number of required shape parameters. Second, as point measurements from one part of the shape also contain information about the symmetric counterparts the estimator becomes more robust against occlusions. However, symmetric transformations have to be applied carefully, as they may produce unintended side effects in the measurement model.

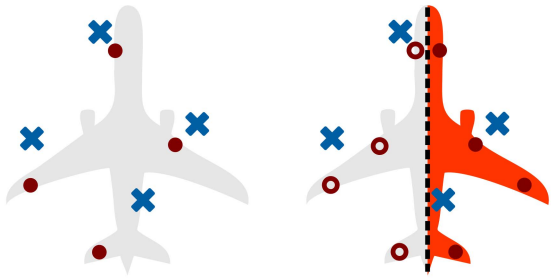

Fig. 1. Common tracking algorithms (a) require a generative model for measurements (blue crosses) that considers sources (red filled circles) over the entire shape. The proposed approach (b) only requires modeling sources in a non-redundant part (orange), so that the rest (red empty circles) of the shape follows from symmetry.

Fig. 1 illustrates the key idea of incorporating symmetry. While common tracking approaches assume measurements originating from sources on the entire airplane (Fig. 1(a)), we propose to model measurement sources just on a single side of the shape (orange), and obtain the rest by mirroring (Fig. 1(b)) in this case. We will denote this orange region as the *non-redundant part* of the shape.

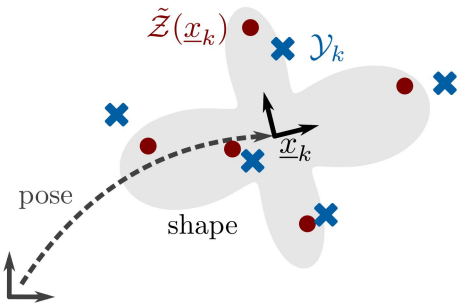

Fig. 2. *Given*: Noisy point measurements $\mathcal{Y}_k$ of sources $\tilde{\mathcal{Z}}(\underline{x}_k)$ on the object, measured at time k. *Desired*: Object parameters $\underline{x}_k$ for the specified model.

Our intention is to explore how different generative models as commonly used in Bayesian extended object tracking can take advantage of these symmetric considerations. Specifically, we will focus on Spatial Distribution Models [9], [24], Greedy Association Models [4], [7] as used in curve fitting, and Random Hypersurface Models [1–3], [6]. Sample-based filtering techniques [10], [23] will be used for implementation.

There are many related approaches that exploit geometric symmetries, e.g., surveyed in [16] and [17]. In the context of [17], our work would be classified as *model acquisition and representation*. Related work on tracking is proposed in [8], where random matrices are used to describe ellipsoidal and non-ellipsoidal [13] extended objects which produce measurement sources according to a known distribution. In [15], reflectional symmetry is incorporated into an image-based tracking algorithm that estimates the bounding box of a moving symmetric object. Reflectional symmetry has also been exploited for segmentation purposes [19]. Simplifying a symmetric mesh was proposed in [22], where the authors incorporate symmetry in the data structure of the mesh in order to remove redundancies. In [20], the authors even proceed one step further by generating a complex shape by back-projecting silhouettes. Treating symmetric multimodalities with directional statistics [12] is also a related field of research, as well as symmetric measurement functions [14] that consider symmetry in the sense of invariance to switching specific parts of the state vector. Note that, while other approaches which exploit geometric symmetries mostly work with image sequences of the object, we only use sparse point measurements. As such, and to the best of our knowledge, this is the first approach to explicitly incorporate geometric symmetries into Bayesian extended object tracking.

The paper is structured as follows. In Sec. 2, the mathematical problem is stated and the model parameters are introduced. Bayesian extended object tracking is discussed in Sec. 4, followed by the key idea of our approach in Sec. 5. For the considered symmetries, as explained in Sec. 6, simplification is further elaborated in Sec. 7 in order to derive a general simplification scheme. The implementation of the proposed approach then is described in Sec. 8. We illustrate these concepts by deriving symmetric models for sticks (Sec. 9) and symmetric star-convex shapes (Sec. 10). These models are evaluated in Sec. 11 and compared against their non-simplified paragons. Finally, conclusions are drawn in Sec. 12.

2 PROBLEM STATEMENT

Tracking an extended object consists of estimating the object state $\underline{x}_k$ as a combination of pose (position and orientation) and shape parameters[1]

$$\underline{x}_k = \begin{bmatrix} \underline{x}_k^{\text{pose}} \\ \underline{x}_k^{\text{shape}} \end{bmatrix}, \tag{1}$$

at each time step k, based on a list of n_k given noisy point observations

$$\mathcal{Y}_k = \{\underline{y}_{i,k} \mid i = 1,\ldots,n_k\} \tag{2}$$

from the object. In general, the dimension d of these points is two or three. The potentially time-varying number n_k of measurements is considered to not contain any information about the object extent. We assume that the measurements originate from source points $\tilde{\underline{z}}_{i,k} \in \tilde{\mathcal{Z}}(\underline{x}_k)$ on the object corrupted by noise in the form

$$\underline{y}_{i,k} = \tilde{\underline{z}}_{i,k} + \underline{w}_{i,k}. \tag{3}$$

The additive noise term $\underline{w}_{i,k}$ is assumed to be drawn from the zero-mean Gaussian distribution $p(\underline{w}_{i,k}) = \mathcal{N}(\underline{0}, \mathbf{C}_{\underline{w}_{i,k}})$, and assumed to be independent from the state and the measurement source. In the following, we denote the set of all possible measurement sources $\tilde{\mathcal{Z}}(\underline{x}_k)$ as the *shape* of the object. Fig. 2 shows a sketch of the estimation task and involved parameters. Note that i) considerations on clutter measurements are not included in this paper, and ii) time indices k and measurement indices i will be dropped when not needed.

2.1 Separation of Shape and Pose

In order to keep geometric considerations simple, we separate pose and shape by using two coordinate frames (see Fig. 2): the *object frame* that represents the object without any pose information, i.e., unrotated and centered on the origin, and the *world frame* that represents how the object is seen from the outside. The function H transforms a given point $\underline{z}^W$, given in the world frame, to the point $\underline{z}^O$ in the object frame, by means of the rigid transformation

$$\underline{z}^O = H(\underline{x}, \underline{z}^W) = \mathbf{R} \cdot \underline{z}^W + \underline{t}, \tag{4}$$

where $\mathbf{R}$ is a rotation matrix and $\underline{t}$ is a translation vector, both derived from $\underline{x}$. Unless otherwise stated, all geometric considerations are assumed to refer to the object frame.

[1] Note that the state can easily be extended to include further parameters.

3 NOTATION

We denote vectors with underline $\underline{x}$ and matrices with capital bold letters $\mathbf{C}$.

$\underline{x}$	object state vector
$\underline{z}$	points $\underline{z} \in \mathbb{R}^d$ in Cartesian coordinates
$\tilde{\mathcal{Z}}(\underline{x})$	shape of the object (set of all measurement sources $\tilde{\underline{z}} \in \tilde{\mathcal{Z}}(\underline{x})$) for a given state $\underline{x}$
$\tilde{\underline{z}}(\underline{x}, s)$	measurement sources $\tilde{\underline{z}} \in \tilde{\mathcal{Z}}(\underline{x})$ in function of the state $\underline{x}$ and index parameters s
$\tilde{\mathcal{Z}}(\underline{x}, t)$	subshapes $\tilde{\mathcal{Z}}(\underline{x}, t) \subseteq \tilde{\mathcal{Z}}(\underline{x})$ in function of an index parameter t
$\mathcal{Y}$	list of measurements $\underline{y}$
$p(\underline{x})$	prior distribution of the object state
$p(\underline{y} \mid \underline{x})$	likelihood for the single measurement $\underline{y}$
$p(\underline{z} \mid \underline{x})$	distribution of points $\underline{z} \in \mathbb{R}^d$ to be measurement sources, given the state $\underline{x}$,
$g(\underline{x}, \underline{z})$	shape function that relates points $\underline{z}$ to the shape $\tilde{\mathcal{Z}}(\underline{x})$
$T(\underline{z})$	aggregation function that maps points $\underline{z}$ to the non-redundant part
$\mathcal{N}(\underline{z}; \underline{\mu}, \mathbf{C})$	Gaussian distribution with mean $\underline{\mu}$, covariance matrix $\mathbf{C}$, evaluated at $\underline{z}$

4 BAYESIAN EXTENDED OBJECT TRACKING

In this section, we introduce the concepts of Bayesian extended object tracking. In a Bayesian estimator, the state $\underline{x}$ to be estimated is modeled as a random vector whose distribution $p(\underline{x})$ represents the uncertain knowledge about the object's pose and shape. In this work, we assume this uncertainty to be Gaussian.

The tracking algorithm consists of two alternating steps. First, the *prediction step* lets the distribution $p(\underline{x})$ evolve over time according to a system model. Second, the *measurement update step* incorporates new measurement points $\mathcal{Y}$ according to Bayes' rule

$$p(\underline{x} \mid \mathcal{Y}) \propto p(\mathcal{Y} \mid \underline{x}) \cdot p(\underline{x}), \tag{5}$$

where $p(\mathcal{Y} \mid \underline{x})$ is the likelihood that describes how likely a measured set of points $\mathcal{Y}$ is, given a state $\underline{x}$.

As we assume all points $\underline{y}_i \in \mathcal{Y}$ to be conditionally independent from the state $\underline{x}$, the likelihood can be rewritten to

$$p(\mathcal{Y} \mid \underline{x}) = \prod_{i=1}^{n} p(\underline{y}_i \mid \underline{x}), \tag{6}$$

which lets us consider individual likelihoods for single measurements $\underline{y}_i \in \mathcal{Y}$. If more points are available, they can be processed sequentially according to (6).

Furthermore, as the measurement noise is assumed to be independent from the state, the likelihood $p(\underline{y} \mid \underline{x})$ can be divided into

$$p(\underline{y} \mid \underline{x}) = \int_{\mathbb{R}^d} p(\underline{y} \mid \underline{z}) \cdot p(\underline{z} \mid \underline{x}) d\underline{z}, \tag{7}$$

where the *sensor model* $p(\underline{y} \mid \underline{z})$ specifies the distribution of measurements $\underline{y}$ for a given point $\underline{z}$, and the *source model* $p(\underline{z} \mid \underline{x})$ specifies the distribution of points $\underline{z} \in \mathbb{R}^d$ to be the measurement sources for a given state $\underline{x}$. Both are schematically shown in Fig. 3.

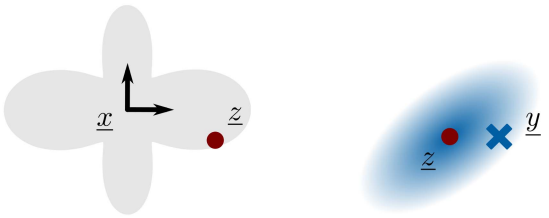

(a) source model $p(\underline{z}|\underline{x})$ (b) sensor model $p(\underline{y}|\underline{z})$

Fig. 3. Sketch of source model and sensor model.

According to (3), the sensor model is immediately given by the convolution

$$\begin{aligned} p(\underline{y} \mid \underline{z}) &= \int_{\mathbb{R}^d} p(\underline{y} \mid \underline{z}, \underline{w}) \cdot p(\underline{w}) d\underline{w} \\ &= \int_{\mathbb{R}^d} \delta(\underline{y} - (\underline{z} + \underline{w})) \cdot \mathcal{N}(\underline{w}; \underline{0}, \mathbf{C}_w) d\underline{w} \\ &= \mathcal{N}(\underline{y} - \underline{z}; \underline{0}, \mathbf{C}_w) \end{aligned} \tag{8}$$

For the source model, in cases where the true source is known, e.g., when looking at point objects without extent, it holds that $p(\underline{z} \mid \underline{x}) = \delta(\underline{z} - \tilde{\underline{z}}(\underline{x}))$, where $\tilde{\underline{z}}(\underline{x})$ refers to the source location of the point object. However, as we consider extended objects in this work, each state $\underline{x}$ generates a set of possible sources $\tilde{\mathcal{Z}}(\underline{x})$ rather than a single source. In order to allow more than one measurement source, we introduce $s \in \mathcal{S}$ as an index parameter that iterates through all possible sources $\tilde{\underline{z}}(\underline{x}, s) \in \tilde{\mathcal{Z}}(\underline{x})$ for a given state $\underline{x}$. The parameter s often refers to real-valued scalars from $\mathcal{S} \subseteq \mathbb{R}$ which, e.g., allows for iterating through sources along a line segment. However, in the case of sources on more complex shapes, such as a rectangle, the index parameter can be vector-valued. For example, in Sec. 4.3, we use a parametrization based on two index parameters $s \in \mathcal{S}$, and $t \in \mathcal{T}$, where pairs of (s, t) iterate through the sources $\tilde{\underline{z}}(\underline{x}, s, t) \in \tilde{\mathcal{Z}}(\underline{x})$.

An appropriate source model for extended objects has the form $p(\underline{z} \mid \underline{x}, s) = \delta(\underline{z} - \tilde{\underline{z}}(\underline{x}, s))$, which additionally depends on the index parameter s, and each refers to a single source. The task then is to derive a source model $p(\underline{z} \mid \underline{x})$ based on the individual source models $p(\underline{z} \mid \underline{x}, s)$. As the true s is usually not known in advance, we are faced with the so called *association problem*. In the following, we summarize three popular source models that deal with this problem. Accompanying the textual description, Fig. 4 presents some illustrative examples.

4.1 Spatial Distribution Model

A *spatial distribution model* (SDM) as presented in [9], [24] is a source model $p(\underline{z} \mid \underline{x})$, derived by marginalizing $s \in \mathcal{S}$ out of the individual models $p(\underline{z} \mid \underline{x}, s)$. The intuition of an SDM is to *explicitly* assign a probabil-

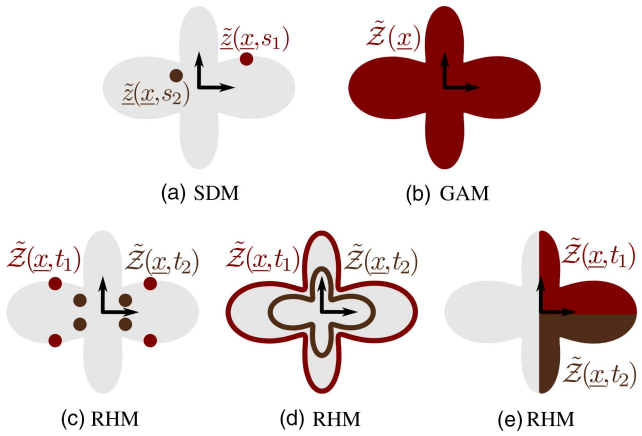

Fig. 4. Sketch of the considered types of source models.

ity $p(s)$ to each individual source $\tilde{\underline{z}}(\underline{x},s) \in \tilde{\mathcal{Z}}(\underline{x})$ of being measured. The marginalization then can be written as

$$p(\underline{z} \mid \underline{x}) = \int_{\mathcal{S}} p(\underline{z} \mid \underline{x},s) \cdot p(s) ds \qquad (9)$$
$$= \int_{\mathcal{S}} \delta(\underline{z} - \tilde{\underline{z}}(x,s)) \cdot p(s) ds.$$

In other words, each potential source $\tilde{\underline{z}}(\underline{x},s)$ is considered as hypothesis and weighted according to its probability.

A popular reformulation [9], [24] of (9) is to substitute the expression $\underline{z} - \tilde{\underline{z}}(\underline{x},s)$ by a distance-related function $\|\underline{z} - \tilde{\underline{z}}(\underline{x},s)\|$ that returns a scalar 0 if $\underline{z}$ equals $\tilde{\underline{z}}(\underline{x},s)$. By means of the distance function, the SDM (9) can be rewritten as

$$p(\underline{z} \mid \underline{x}) = \int_{\mathcal{S}} \delta(\|\underline{z} - \tilde{\underline{z}}(\underline{x},s)\|) \cdot p(s) ds. \qquad (10)$$

A drawback of the SDM is that in most real-life scenarios, $p(s)$ is not known in advance, and deriving it is a non-trivial task, as it depends on factors such as sensor to object geometry, the specific segmentation algorithm, and occlusions, among others. This raises the need for approaches that depend less on $p(s)$.

4.2 Greedy Association Model

Another source modeling technique, popular in curve fitting [7], is to approximate the unknown source distribution by $p(s) = \delta(s - \hat{s})$ where the index $\hat{s}$ specifies the true source. The sifting property then lets us eliminate the integral in (10)

$$p(\underline{z} \mid \underline{x}) = \int_{\mathcal{S}} \delta(\|\underline{z} - \tilde{\underline{z}}(x,s)\|) \cdot \delta(s - \hat{s}) ds \qquad (11)$$
$$= \delta(\|\underline{z} - \tilde{\underline{z}}(x,\hat{s})\|).$$

Although this would be the ideal source model, $\hat{s}$ and in consequence $\tilde{\underline{z}}(x,\hat{s})$ is usually unknown (association problem). As an approximation, $\hat{s}$ can be greedily chosen, such that $\tilde{\underline{z}}(x,\hat{s})$ refers to the source on the shape that is "closest" to $\underline{z}$. In consequence $\|\underline{z} - \tilde{\underline{z}}(x,\hat{s})\|$ returns 0 for all $\underline{z} \in \tilde{\mathcal{Z}}(\underline{x})$. This motivates the use of an *implicit shape function* in the form of

$$g(\underline{x},\underline{z}) = \min_{s \in \mathcal{S}} (\|\underline{z} - \tilde{\underline{z}}(\underline{x},s)\|), \qquad (12)$$

which returns the minimum over all distances between the point $\underline{z}$ and all sources on the shape $\tilde{\mathcal{Z}}(\underline{x})$. Note that finding the minimum implicitly includes the greedy selection of the expected source. Substituting the expression $\|\underline{z} - \tilde{\underline{z}}(x,\hat{s})\|$ in (11) with the shape function $g(\underline{x},\underline{z})$ from (12), we obtain a *Greedy Association Model* (GAM)

$$p(\underline{z} \mid \underline{x}) = \delta(g(\underline{x},\underline{z})). \qquad (13)$$

As an advantage over SDMs, GAMs do not depend on any known distribution $p(s)$ at all, but at the cost of a greedy association. This approximation was shown in [7] to introduce a parameter bias in the estimate in the presence of high noise. A second issue is that estimators using GAMs usually require regularization as they do not penalize overestimates [24].

4.3 Random Hypersurface Model

Combining the ideas from the SDM and the GAM, we arrive at *Random Hypersurface Models* (RHMs) [2] that inherit the advantages from both source models. In detail, they depend less on the distribution of individual sources and do not require regularization. To derive the RHM, let us start with an SDM that is parameterized by two indices $s \in \mathcal{S}$ and $t \in \mathcal{T}$, i.e., pairs (s,t) iterate through all possible sources $\tilde{\underline{z}}(x,s,t) \in \tilde{\mathcal{Z}}(\underline{x})$ for a given state $\underline{x}$. Let each source have a given probability $p(s,t)$. Then, marginalizing (s,t) out of $p(\underline{z} \mid \underline{x},s,t)$ an SDM can be written as

$$p(\underline{z} \mid \underline{x}) = \int_{\mathcal{S}} \int_{\mathcal{T}} p(\underline{z} \mid \underline{x},s,t) \cdot p(s,t) ds\, dt \qquad (14)$$
$$= \int_{\mathcal{S}} \int_{\mathcal{T}} \delta(\|\underline{z} - \tilde{\underline{z}}(x,s,t)\|) \cdot p(s \mid t) \cdot p(t) ds\, dt.$$

The goal of using two indices is to choose their parametrization such that for a given t_i, iterating over all sources $\tilde{\underline{z}}(x,s,t_i)$ with $s \in \mathcal{S}$ refers to a reasonable subshape we denote as $\tilde{\mathcal{Z}}(\underline{x},t_i)$. These subshapes, however, are not unique and can be defined in multiple ways. Three illustrative examples are shown in 4(c–e) and range from subshapes composed of a few discrete points (Fig. 4(c)), over a scaled boundary (Fig. 4(d)) to entire parts of the shape (Fig. 4(e)).

An RHM assumes that $p(t)$ is known in advance (SDM), i.e., the probability that a measurement originates from a specific subshape, while the probability of the individual source on the subshape is unknown and has to be determined greedily according to $p(s \mid t) = \delta(s - \hat{s}_t)$ (GAM). Plugging $p(s \mid t)$ into (10) then lets us eliminate the integral over s

$$p(\underline{z} \mid \underline{x}) = \int_{\mathcal{T}} \delta(\|\underline{z} - \tilde{\underline{z}}(x,\hat{s}_t,t)\|) \cdot p(t) dt. \qquad (15)$$

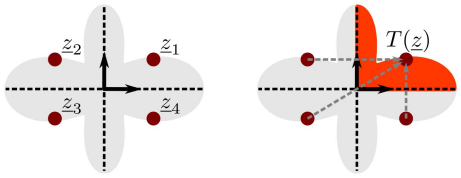

(a) symmetric sources (b) aggregation

Fig. 5. Symmetric points $\underline{z}_1$, $\underline{z}_2$, $\underline{z}_3$, and $\underline{z}_4$ all lie inside or outside of a symmetric shape. The aggregation function $T(\cdot)$ transforms all points $\underline{z}$ to their symmetric equivalents in the the non-redundant part (orange).

Analogously to the GAM, it is common practice [2] to substitute the expression $\|\underline{z} - \tilde{\underline{z}}(x, \hat{s}_t, t)\|$ with an implicit shape function

$$g_t(\underline{x}, \underline{z}) = \min_{s \in \mathcal{S}}(\|\underline{z} - \tilde{\underline{z}}(\underline{x}, s, t)\|) \tag{16}$$

that additionally depends on t and returns the distance to the subshape $\tilde{\mathcal{Z}}(\underline{x}, t)$. Finally, by means of $g_t(\cdot)$, we can rewrite the source model (15) to obtain the RHM

$$p(\underline{z} \mid \underline{x}) = \int_{\mathcal{T}} \delta(g_t(\underline{x}, \underline{z})) \cdot p(t) dt. \tag{17}$$

REMARK 1 **(Set-theoretic Ignorance)**
In this work, we use the term *set-theoretic ignorance* to denote that a source model greedily selects sources from a (sub-)shape instead of assuming an individual probability on each source, as these are assumed to be unknown. As such, SDMs do not assume any set-theoretic ignorance at all, while GAMs assume set-theoretic ignorance over the entire shape. In RHMs, the *degree* of set-theoretic ignorance depends on the extent of the subshapes.

5 KEY IDEA

We will now discuss the key idea of applying symmetric simplification to source models $p(\underline{z} \mid \underline{x})$. While there are many ways to describe symmetries, in this paper we focus on symmetry as *repetition*. As such, a symmetric shape can be seen as being generated by the repeated transformation of a small part of the shape, which we denote as the *non-redundant part*. Then, for these shapes, we can find an *aggregation function* $T(\underline{z})$ that maps each point to its symmetric equivalent in the non-redundant part. More formally, let $T(\cdot)$ be an *idempotent* function, i.e., it always holds that $T(T(\underline{z})) = T(\underline{z})$. We say that a shape $\tilde{\mathcal{Z}}(\underline{x})$ is symmetric by $T(\cdot)$ if for all points $\underline{z} \in \mathbb{R}^d$ it holds that

$$\underline{z} \in \tilde{\mathcal{Z}}(\underline{x}) \Leftrightarrow T(\underline{z}) \in \tilde{\mathcal{Z}}(\underline{x}). \tag{18}$$

In this case, we say that $T(\cdot)$ is an aggregation function of the shape $\tilde{\mathcal{Z}}(\underline{x})$, and its non-redundant part is given by $T(\tilde{\mathcal{Z}}(\underline{x}))$. This relationship is illustrated in Fig. 5 for a 2-axial symmetric shape.

The key idea is to exploit that under certain conditions, the presented source models for symmetric shapes

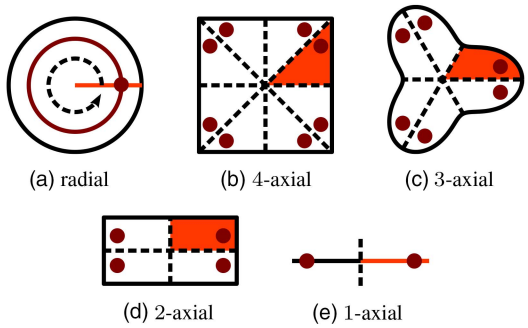

(a) radial (b) 4-axial (c) 3-axial

(d) 2-axial (e) 1-axial

Fig. 6. Types of symmetry: rotational symmetry (a) and instances of axial symmetry (b–e). The non-redundant part of each shape is marked in orange. As an example, one source in each non-redundant part and all symmetric equivalents is marked in red.

are symmetric too, i.e., it holds that

$$p(\underline{z} \mid \underline{x}) = p(T(\underline{z}) \mid \underline{x}). \tag{19}$$

Specifically, we will show that this identity holds when a source model only has symmetric subshapes. Then, by aggregating symmetric points according to $T(\cdot)$, the original domain $\mathbb{R}^d$ of the source model $p(\underline{z} \mid \underline{x})$ can be reduced to the non-redundant part $T(\mathbb{R}^d)$ of the domain. This allows us to specify a source model exclusively in the non-redundant part and use $p(T(\underline{z}) \mid \underline{x})$ in the estimator. The desired simplification for the models in the top row of Fig. 7 is illustrated in the bottom row.

As can be seen, all shape information is contained in the non-redundant part, e.g., the first quadrant for the 2-axial symmetry.

6 CONSIDERED SYMMETRIES

Some shapes with corresponding symmetries are visualized in Fig. 6. The non-redundant part of each shape is marked in orange. In this work, we focus on rotoreflections with $2n$-fold rotation angle, which means a shape is generated by reflecting its non-redundant part with respect to $n \in \mathbb{N}$ rotated axes that intersect in the origin. This type of symmetry includes special cases such as axial symmetries in Fig. 6(b–e), as well as radial symmetry for $n \to \infty$ (see Fig. 6(a)). Next, we derive explicit formulas for appropriate aggregation functions $T(\cdot)$ for two and three dimensions.

6.1 2D Aggregation Function

When dealing with rotoreflections in 2D, polar coordinates offer a convenient representation. For conversion of a point $\underline{z}$, given in Cartesian coordinates $\underline{z} = [z_1, z_2]^{\mathrm{T}}$, the corresponding representation in polar coordinates is defined as

$$\theta(\underline{z}) = \operatorname{atan2}(z_2, z_1), \tag{20}$$

$$r(\underline{z}) = \sqrt{z_1^2 + z_2^2}, \tag{21}$$

where $\theta(\underline{z})$ is the angle to the z_1-axis and $r(\underline{z})$ is the Euclidean norm of $\underline{z}$. For a rotoreflection, its $2n$-fold

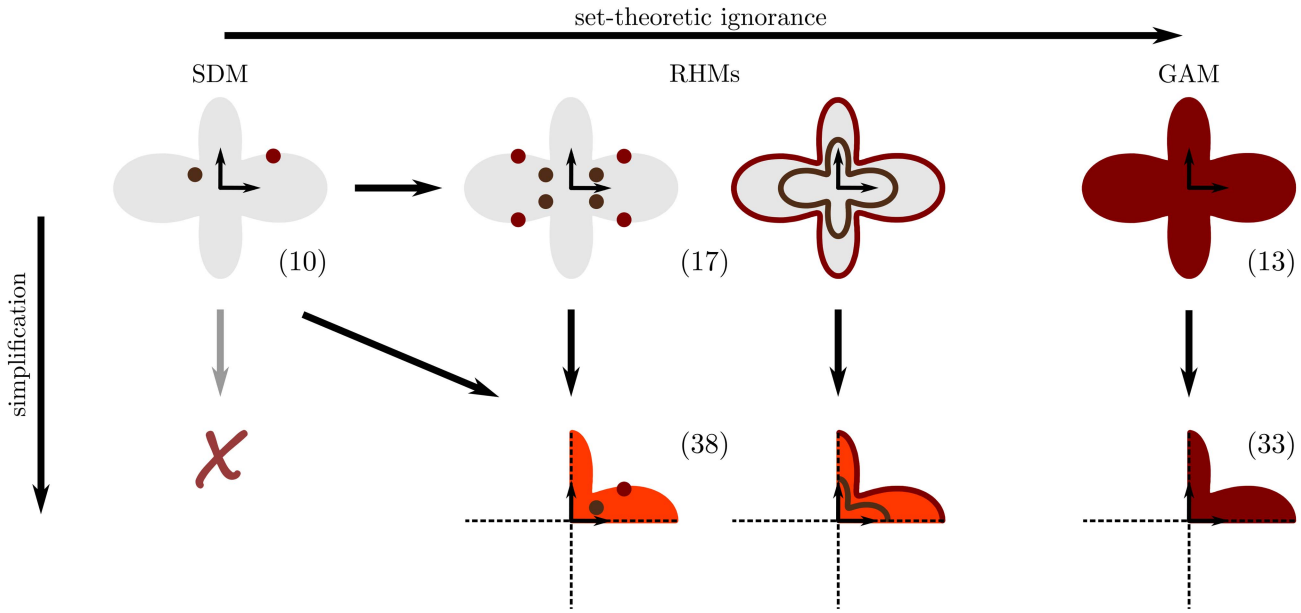

Fig. 7. Overview of the proposed approach. The top row illustrates the considered source models. From the left to the right, the set-theoretic ignorance in the model increases. The bottom row shows the simplified source models for the top row. Sources belonging to the same (sub-)sets of the shape, are colored in brown and red, respectively.

rotation angle is given by

$$\Theta = \frac{\pi}{n}, \tag{22}$$

which means that each of the n axes of symmetry is rotated about Θ. In terms of polar coordinates, we then define the non-redundant part to lie in the period from 0 to Θ. Thus, the corresponding aggregation function $T(\cdot)$ should map all points onto their equivalents in this part. Note that this mapping does not affect the radius $r(\underline{z})$, but rather it requires a modulo operation on the angle $\theta(\underline{z})$ according to

$$\theta(\underline{z},n) = \begin{cases} \mathrm{mod}(\theta(\underline{z}),\Theta) & \text{if } \left\lfloor \frac{\theta(\underline{z})}{\Theta} \right\rfloor \text{ is even} \\ \Theta - \mathrm{mod}(\theta(\underline{z}),\Theta) & \text{if } \left\lfloor \frac{\theta(\underline{z})}{\Theta} \right\rfloor \text{ is odd.} \end{cases} \tag{23}$$

Finally, an appropriate aggregation function can be defined as

$$T(\underline{z}) = \begin{bmatrix} r(\underline{z}) \cdot \cos(\theta(\underline{z},n)) \\ r(\underline{z}) \cdot \sin(\theta(\underline{z},n)) \end{bmatrix}. \tag{24}$$

Special Cases: The general aggregation function (24) for rotoreflections includes several special cases. For example, given a reflectional symmetry with respect to the z_2-axis (see Fig. 6(e)), the non-redundant part is a half-plane, and the aggregation function

$$T(\underline{z}) = [|z_1|, z_2]^{\mathrm{T}} \tag{25}$$

aggregates points $\underline{z}$, according to its absolute values $|.|$ in z_1. Analogously, the aggregation function for a 2-axial symmetry (see Fig. 5 and Fig. 6(d)) maps each point $\underline{z}$ to the first quadrant, according to

$$T(\underline{z}) = [|z_1|, |z_2|]^{\mathrm{T}}. \tag{26}$$

A rotoreflection with $n \to \infty$ axes causes the non-redundant part to collapse into a ray, e.g., the positive z_1-axis, where the aggregation function can be written as

$$T(\underline{z}) = [\|\underline{z}\|, 0]^{\mathrm{T}}, \tag{27}$$

and maps each point $\underline{z}$ to this axis, according to its distance $\|.\|$ to the origin.

6.2 3D Aggregation Function

For rotoreflections in 3D, cylindrical coordinates are chosen. The conversion of a point $\underline{z}$ given in Cartesian coordinates $\underline{z} = [z_1, z_2, z_3]^{\mathrm{T}}$ is very similar to the 2D case. First, (20) can be used to derive polar coordinates from z_1 and z_2 and second, the height component is directly given by z_3. Introducing an additional symmetry in 3D can be achieved by taking the absolute value of z_3. Then, an aggregation function with reflectional symmetry in the height can be defined as

$$T(\underline{z}) = \begin{bmatrix} r(\underline{z}) \cdot \cos(\theta(\underline{z},n)) \\ r(\underline{z}) \cdot \sin(\theta(\underline{z},n)) \\ |z_3| \end{bmatrix}. \tag{28}$$

7 SIMPLIFICATION BASED ON SYMMETRY

In this section, we derive a simplification scheme for the presented source models, given that a target object has a known rotoreflectional symmetry. To achieve this goal, we investigate the symmetric properties of the different models $p(\underline{z} \mid \underline{x})$ and show how to take advantage of it. In doing so, we begin with the GAM, which allows for the simplest simplification, and subsequently look at the RHM and the SDM.

7.1 Simplified Greedy Association Model

Let the source model of an object with state $\underline{x}$ and shape function $g(\cdot)$ be specified by the GAM $p(\underline{z} \mid \underline{x}) = \delta(g(\underline{x},\underline{z}))$. Further, let the object shape have a known rotoreflectional symmetry described by the aggregation function $T(\cdot)$. Examining the symmetric properties of this source model refers to examining those of the shape function. As $g(\cdot)$ returns the minimum distance from points $\underline{z} \in \mathbb{R}^d$ to the shape $\tilde{\mathcal{Z}}(\underline{x})$, it produces equal values for all symmetric equivalents of $\underline{z}$. Specifically, it holds that

$$\begin{aligned} g(\underline{x},\underline{z}) &= \min_{s\in\mathcal{S}}(\|\underline{z} - \tilde{\underline{z}}(\underline{x},s)\|) \\ &= \min_{s\in\mathcal{S}}(\|T(\underline{z}) - \tilde{\underline{z}}(\underline{x},s)\|) \\ &= g(\underline{x},T(\underline{z})), \end{aligned} \tag{29}$$

which immediately implies that the GAM (13)

$$p(\underline{z} \mid \underline{x}) = \delta(g(\underline{x},\underline{z})) = \delta(g(\underline{x},T(\underline{z}))) = p(T(\underline{z}) \mid \underline{x}) \tag{30}$$

is symmetric too. From this follows that in practice the shape function $g(\cdot)$ needs to be evaluated only in the non-redundant part $T(\mathbb{R}^d)$ of the domain $\mathbb{R}^d$.

As simplification, we propose to substitute the original shape function $g(\cdot)$ with a simplified shape function $g^*(\cdot)$, which is exclusively defined in the non-redundant part of the domain. For this purpose, let the indices $s^* \in \mathcal{S}^*$ with $\mathcal{S}^* \subseteq \mathcal{S}$ refer to sources in the non-redundant part $\tilde{\underline{z}}(\underline{x},s^*) \in T(\tilde{\mathcal{Z}}(\underline{x}))$ according to

$$\mathcal{S}^* := \{s \in \mathcal{S} \mid T(\tilde{\underline{z}}(\underline{x},s)) = \tilde{\underline{z}}(\underline{x},s)\}. \tag{31}$$

Then a simplified shape function is given by

$$g^*(\underline{x},\underline{z}) := \min_{s^*\in\mathcal{S}^*}(\|T(\underline{z}) - \tilde{\underline{z}}(\underline{x},s^*)\|) \tag{32}$$

that internally performs the aggregation $T(\cdot)$ and can be employed to define a simplified GAM

$$p(\underline{z} \mid \underline{x}) = \delta(g^*(\underline{x},\underline{z})). \tag{33}$$

Note that this simplification does not introduce any error at all in the source model, as it only exploits the fact that distances from symmetric points to a symmetric shape are equal. For this reason, we can encapsulate all symmetric considerations in the shape function.

7.2 Simplified Random Hypersurface Model

Let the source model $p(\underline{z} \mid \underline{x})$ of an object $\underline{x}$ with shape function $g_t(\cdot)$ and distribution $p(t)$ be specified by the RHM (17). This means that the shape is composed of subshapes $\tilde{\mathcal{Z}}(\underline{x},t)$, where each of them is specified by the shape function $g_t(\cdot)$. Furthermore, let the object shape have a known rotoreflectional symmetry described by the aggregation function $T(\cdot)$. In order to apply symmetric simplification, we require each of the subshapes $\tilde{\mathcal{Z}}(\underline{x},t)$ to be symmetric with respect to a given aggregation function $T(\cdot)$, i.e., for all points $\underline{z}$ it shall hold that

$$\underline{z} \in \tilde{\mathcal{Z}}(\underline{x},t) \Leftrightarrow T(\underline{z}) \in \tilde{\mathcal{Z}}(\underline{x},t). \tag{34}$$

When looking at the example RHMs from Fig. 4, subshapes in (c) and (d) are symmetric, while the subshapes in (e) are not. Then, all symmetric considerations (29) from the GAM apply to the symmetric subshapes $\tilde{\mathcal{Z}}(\underline{x},t)$ and yield the identity

$$g_t(\underline{x},\underline{z}) = g_t(\underline{x},T(\underline{z})). \tag{35}$$

From this can be concluded that, given all subshapes are symmetric, the RHM (17)

$$\begin{aligned} p(\underline{z} \mid \underline{x}) &= \int_{\mathcal{T}} \delta(g_t(\underline{x},\underline{z})) \cdot p(t)dt \\ &= \int_{\mathcal{T}} \delta(g_t(\underline{x},T(\underline{z}))) \cdot p(t)dt \\ &= p(T(\underline{z}) \mid \underline{x}) \end{aligned} \tag{36}$$

is also symmetric. In turn, the shape function $g_t(\cdot)$ needs to be evaluated only in the non-redundant part of the domain $T(\mathbb{R}^d)$, which gives rise to the same simplification technique as applied to the GAM. We propose to substitute the original shape function $g_t(\cdot)$ with a simplified version

$$g_t^*(\underline{x},\underline{z}) := \min_{s^*\in\mathcal{S}^*}(\|T(\underline{z}) - \tilde{\underline{z}}(\underline{x},s^*,t)\|) \tag{37}$$

that only needs to be evaluated in the non-redundant domain $T(\mathbb{R}^d)$. Then, the simplified RHM is given by

$$p(\underline{z} \mid \underline{x}) = \int_{\mathcal{T}} \delta(g_t^*(\underline{x},\underline{z})) \cdot p(t)dt. \tag{38}$$

Again, this simplification does not introduce any error at all, as it only exploits the fact that distances from symmetric points to a symmetric (sub-)shape are equal.

7.3 Simplified Spatial Distribution Model

Let the source model $p(\underline{z} \mid \underline{x})$ of an object with $\underline{x}$ with distribution $p(s)$ over the sources $\tilde{\underline{z}}(\underline{x},s)$ be specified by the SDM (10). Furthermore, let the object shape have a known rotoreflectional symmetry described by the aggregation function $T(\cdot)$. It can be seen that for (10) in general $p(\underline{z} \mid \underline{x})$ and $p(T(\underline{z}) \mid \underline{x})$ do not produce identical results as

$$\|\underline{z} - \tilde{\underline{z}}(\underline{x},s)\| \neq \|T(\underline{z}) - \tilde{\underline{z}}(\underline{x},s)\|. \tag{39}$$

In consequence, an SDM as defined in (10) cannot be simplified using the proposed technique, which is indicated in Fig. 7. In order to allow for simplification, we propose to approximate the SDM by an RHM that uses symmetric subshapes and then simplify this RHM.

Creating Symmetric Subshapes: We can use $T(\cdot)$ to create symmetric subshapes by taking a source $\tilde{\underline{z}}(\underline{x},s^*)$ with $s^* \in \mathcal{S}^*$ that lies in the non-redundant part and then collect all sources $T(\tilde{\underline{z}}(\underline{x},s))$ being mapped to this source. We denote the corresponding subshape as $\tilde{\mathcal{Z}}(\underline{x},s^*)$ and define the *equivalence class* of indices, which contains the indices of all sources in the subshape according to

$$[s^*] := \{s \in \mathcal{S} \mid T(\tilde{\underline{z}}(\underline{x},s)) = \tilde{\underline{z}}(\underline{x},s^*)\}. \tag{40}$$

The illustration of the left RHM in the first row of Fig. 7 shows an example of these subshapes. Note that per definition, only a single point of each subshape lies in the non-redundant part (see Fig. 6). Based on these subshapes, the original SDM (10) can now be approximated by an RHM.

Approximating SDM by RHM: In order to define the desired RHM, we need to specify a shape function $g_{s^*}(\underline{x},\underline{z})$ that returns the minimum distance from a point $\underline{z}$ to a subshape $\tilde{\mathcal{Z}}(\underline{x},s^*)$, as well as the distribution $p(s^*)$. An appropriate shape function is given by

$$g_{s^*}(\underline{x},\underline{z}) = \min_{s\in[s^*]}(\|\underline{z}-\tilde{\underline{z}}(\underline{x},s)\|). \tag{41}$$

The distribution $p(s^*)$ specifies the probability that a source within the subshape $\tilde{\mathcal{Z}}(\underline{x},s^*)$ is measured and can be calculated by integrating the individual probabilities according to

$$p(s^*) = \int_{[s^*]} p(s)ds. \tag{42}$$

Using the shape function g_{s^*} and the distribution $p(s^*)$ the RHM from (17) can then be rewritten to

$$p(\underline{z}\mid\underline{x}) = \int_{\mathcal{S}^*} \delta(g_{s^*}(\underline{x},\underline{z}))\cdot p(s^*)ds^*. \tag{43}$$

Simplifying the RHM: At this point, we arrived at an RHM that uses symmetric subshapes, which in turn lets us substitute the original shape function $g_{s^*}(\cdot)$ with a simplified version

$$g^*_{s^*}(\underline{x},\underline{z}) = \|T(\underline{z})-\tilde{\underline{z}}(\underline{x},s^*)\| \tag{44}$$

that only needs to be evaluated in the non-redundant part $T(\mathbb{R}^d)$ of the domain $\mathbb{R}^d$. We will denote (43) as simplified SDM.

When comparing the simplified SDM (43) to the original SDM (10), there are two differences. First, the aggregation of symmetric sources has introduced a set-theoretic ignorance, as the model only allows distinct probabilities for subshapes $\tilde{\mathcal{Z}}(\underline{x},s^*)$, where sources in the subshapes are associated greedily. Second, the integration variable s^* of the RHM has a reduced domain compared to the original integration variable s of the SDM. When using a sample-based filter, this reduction yields a higher effective sample resolution, which improves the estimation result.

It is important to note that, in practice, the simplified source models in the bottom row of Fig. 7 can be used directly without having to model the traditional versions from the top row.

8 DERIVING THE ESTIMATOR

We will now derive a Bayesian estimator that takes advantage of the symmetric considerations of the previous section. For this purpose, we derive likelihoods based on the simplified source models and then show how the measurement update can be implemented using a *Linear Regression Kalman Filter*.

8.1 Likelihoods and Measurement Equations

In a preliminary step, let us plug the sensor model (8) in the likelihood from (7) and rearrange it to

$$\begin{aligned} p(\underline{y}\mid\underline{x}) &= \int_{\mathbb{R}^d}\int_{\mathbb{R}^d} p(\underline{y}\mid\underline{z},\underline{w})\cdot p(\underline{w})d\underline{w}\,p(\underline{z}\mid\underline{x})d\underline{z} \\ &= \int_{\mathbb{R}^d}\int_{\mathbb{R}^d} \delta((\underline{y}-\underline{w})-\underline{z})\cdot p(\underline{w})d\underline{w}\cdot p(\underline{z}\mid\underline{x})d\underline{z}. \end{aligned} \tag{45}$$

As a reminder, $\underline{y}$ is a point measurement and $\underline{w}$ is a noise variable which describes the sensor uncertainty. Then, as in the previous section, we begin our considerations with the simplest model, i.e., the GAM. Plugging the simplified GAM $p(\underline{z}\mid\underline{x})$ from (33) into the rearranged likelihood (45) yields

$$\begin{aligned} p(\underline{y}\mid\underline{x}) &= \int_{\mathbb{R}^d}\int_{\mathbb{R}^d} \delta((\underline{y}-\underline{w})-\underline{z})\cdot p(\underline{w})d\underline{w}\cdot\delta(g^*(\underline{x},\underline{z}))d\underline{z} \\ &= \int_{\mathbb{R}^d} \delta(g^*(\underline{x},\underline{y}-\underline{w}))\cdot p(\underline{w})d\underline{w}, \end{aligned} \tag{46}$$

where the integral over $\underline{z}$ was eliminated by applying the sifting property. Again, it is important to note that all symmetric considerations are encapsulated in the simplified shape function $g^*(\cdot)$ that internally applies the aggregation function to $\underline{y}-\underline{w}$ in order to calculate its distance to the shape.

Usually, the shape function $g^*(\cdot)$ will be defined in object coordinates while measurement minus noise $(\underline{y}-\underline{w})^W$ is given in world coordinates. In order to deal with this issue, the conversion technique from (4) can be applied $(\underline{y}-\underline{w})^O = H(\underline{x},(\underline{y}-\underline{w})^W)$. Then, the likelihood can be written as

$$p(\underline{y}\mid\underline{x}) = \int_{\mathbb{R}^d} \delta(h(\underline{x},\underline{y},\underline{w}))\cdot p(\underline{w})d\underline{w}, \tag{47}$$

where h defines a nonlinear *implicit measurement equation* of the form

$$0 = h(\underline{x},\underline{y},\underline{w}) := g^*(\underline{x},H(\underline{x},\underline{y}-\underline{w})). \tag{48}$$

Within this implicit function, the original measurement $\underline{y}$ acts as an additional function parameter, $\underline{w}$ is a non-additive noise variable, and 0 is an artificial pseudo-measurement.

Likewise, the likelihood based on the simplified RHM (33) can be derived as

$$p(\underline{y}\mid\underline{x}) = \int_{\mathbb{R}^d}\int_{\mathcal{T}} \delta(h(\underline{x},\underline{y},\underline{w},t))\cdot p(t)\cdot p(\underline{w})d\underline{w}\,dt. \tag{49}$$

In this case, the implicit measurement equation

$$0 = h(\underline{x},\underline{y},\underline{w},t) := g^*_t(\underline{x},H(\underline{x},\underline{y}-\underline{w}))) \tag{50}$$

additionally depends on a second non-additive noise variable t. Substituting t with s^* in the formulas (49) and (50) yields the simplified SDM.

Unfortunately, it is usually not possible to evaluate the required integrals in the likelihoods and, in turn, the *measurement update step* analytically. Still, there are

techniques available that can be applied in order to derive an approximate update, such as, e.g., *Monte Carlo* integration [9], [18]. Of particular interest are Linear Regression Kalman Filters (LRKF) such as the *Unscented Kalman Filter* (UKF) [10], or the *Smart Sampling Kalman Filter* (S^2KF) [23], which were successfully applied to extended object tracking [1–4], [6].

8.2 Linear Regression Kalman Filter

We now provide instructions and formulas to implement an approximate sample-based Bayes' update [10], [23] for a (simplified) RHM. Alg. 1 shows the resulting Kalman formulas, where the measurement mean μ_h, measurement covariance $\mathbf{C}_h$ and state-measurement cross-covariance $\mathbf{C}_{xh}$ are obtained through deterministic sampling (statistical linearization). It is important to note that besides state $\underline{x}$ and measurement noise $\underline{w}$, the index t is modeled as a random variable and, thus, subject to sampling. This algorithm can easily be adjusted to derive updates for (simplified) GAMs and SDMs by either dropping the noise parameter t or substituting it by s^*.

ALGORITHM 1 *Sample-based Bayes' update for a (simplified) RHM.*

input: prior distribution of state $p(\underline{x})$, and noise $p(\underline{w})$, $p(t)$, measured point $\underline{y}$
output: posterior distribution of state $p(\underline{x}^e)$
begin
draw L samples $\{[\underline{x}_l^{\mathrm{T}}, \underline{w}_l^{\mathrm{T}}, t_l]^{\mathrm{T}}\}_{l=1}^{L}$ from the joint distribution $p([\underline{x}^{\mathrm{T}}, \underline{w}^{\mathrm{T}}, t]^{\mathrm{T}})$;
calculate sample mean μ_h, sample covariance $\mathbf{C}_h$ and sample cross-covariance $\mathbf{C}_{xh}$ according to

$$\mu_h = \frac{1}{L}\sum_{l=1}^{L} h(\underline{x}_l, \underline{y}, \underline{w}_l, t_l),$$

$$\mathbf{C}_h = \frac{1}{L}\sum_{l=1}^{L} h(\underline{x}_l, \underline{y}, \underline{w}_l, t_l)^2 - \mu_h^2,$$

$$\mathbf{C}_{xh} = \frac{1}{L}\sum_{l=1}^{L} (h(\underline{x}_l, \underline{y}, \underline{w}_l, t_l) - \mu_h) \cdot (\underline{x}_l - \mu_x)^{\mathrm{T}};$$

calculate posterior

$$\underline{\mu}_x^e = \underline{\mu}_x + \mathbf{K}\mu_h$$
$$\mathbf{C}_x^e = \mathbf{C}_x - \mathbf{K}\mathbf{C}_h\mathbf{K}^{\mathrm{T}}$$

with Kalman gain $\mathbf{K} = \mathbf{C}_{xh}\mathbf{C}_h^{-1}$;
return $p(\underline{x}^e) = \mathcal{N}(\underline{\mu}_x^e, \mathbf{C}_x^e)$
end

8.3 Discussion

Based on these derivations, we can conclude several remarks.

REMARK 2 **(Usability)**
As all symmetric considerations are encapsulated in the shape function, the proposed simplification approach does not require any adaptions to the filter being used. In consequence, Alg. 1 can be applied to derive the measurement update, using the common source models as well as their simplified versions, simply by switching the measurement function.

REMARK 3 **(Generalization)**
The proposed approach is a general solution to exploit symmetries in the measurement function and is not restricted to shape estimation. Specifically, whenever an implicit measurement equation of the structure

$$\underline{0} = h(\underline{x}, \underline{\alpha}) \tag{51}$$

is given, and for all $\underline{\alpha}$ the identity

$$h(\underline{x}, \underline{\alpha}) = h(\underline{x}, T(\underline{\alpha})) \tag{52}$$

holds, then $h(\cdot)$ can immediately be substituted by an alternative function $h^*(\cdot)$ that only needs to be defined in a reduced domain $T(\cdot)$.

For example, if the shape color is symmetric with respect to the object geometry, we can easily add a color vector $\underline{c}$ to a spatial point vector $\underline{z}$ and apply aggregation in the form of $T([\underline{z}^{\mathrm{T}}, \underline{c}^{\mathrm{T}}]^{\mathrm{T}})$ that maps the spatial dimensions to its equivalent in the non-redundant part while leaving the color untouched. This generalization also applies to measurements related to curvature or other features, as long as they are symmetric with respect to the object geometry.

REMARK 4 **(Benefits)**
The proposed approach allows for modeling an entire shape by solely specifying it in the non-redundant part of the domain, which then is "unfolded" to obtain the entire domain. In turn, each measurement forces the estimator to adjust the shape in the entire domain. Depending on the specific source model, shape, and its parametrization, symmetric simplification allows for

- introducing symmetry constraints upon the estimated shape,
- modeling a more detailed shape while maintaining or even reducing the number of shape parameters,
- reducing the overall complexity by reducing the domain of integration variables, and
- increasing robustness against partial occlusion.

Next, we demonstrate the proposed approach by means of two illustrative examples.

9 EXAMPLE 1: STICK OBJECT

A stick object is a one-dimensional line segment, usually embedded in a higher-dimensional space. We will first derive a simplified source model for the one-dimensional space, and then show a straightforward way to extend this model into higher dimensional space. According to (1), the state $\underline{x}$ of an object is separated into pose $\underline{x}^{\mathrm{pose}}$ and shape $\underline{x}^{\mathrm{shape}}$. For the source model, the stick is modeled as being centered on the origin. Pose will be incorporated in the measurement function.

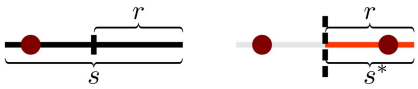

(a) common (b) proposed

Fig. 8. Difference between modeling the stick without (a) and with (b) symmetry.

The only required shape parameter refers to the size of the stick, which is represented by the distance $\underline{x}^{\text{shape}} = r$ from the center to the edge, i.e., $2 \cdot r$ is the stick length.

9.1 No Symmetry

Common approaches [1], [9], [24] use an SDM (9) for the stick (see Fig. 8(a)), where the shape $\tilde{\mathcal{Z}}(\underline{x})$ is parameterized by the sources

$$\tilde{z}(\underline{x}, s) = s \cdot r \tag{53}$$

with $s \in [-1, 1]$. Within this parametrization $\tilde{z}(\underline{x}, -1) = -r$ specifies the left edge of the stick, and $\tilde{z}(\underline{x}, 1) = r$ specifies the right edge, respectively. If the sources are assumed to be uniformly distributed along the stick, the parameter s follows a uniform distribution $p(s) = \mathcal{U}[-1, 1]$. A measurement function is then given by

$$h(\underline{x}, y, w, s) = H(\underline{x}, (y - w)) - s \cdot r, \tag{54}$$

where $H(\underline{x}, (y - w))$ converts points $y - w$ to object coordinates. Even though this model is simple, it has the drawback that estimators based on the linear Gaussian assumption [10], [23] are not capable to estimate r when simultaneously estimating the pose [1], as an effect of the linearization. They propose a *quadratic extension*, in order to design a modified measurement function that overcomes this issue. However, even this approach only works when using advanced filters such as the S^{2}KF [23].

9.2 1-axial Symmetry

We now propose a novel model that can be used for simultaneously estimating shape and pose even with a standard UKF [10]. This model can be obtained by approximating the common SDM by a simplified SDM, which exploits the 1-axial symmetry of the stick.

Specifying Aggregation Function: This symmetry can be described by the aggregation function $T(z) = |z|$ as for all sources $\tilde{z}(\underline{x}, s)$ on the stick, it follows that $|\tilde{z}(\underline{x}, s)|$ also lies on the stick. Based on $T(\cdot)$, the non-redundant part of the stick then falls on the positive z-axis, where the sources are indexed by $\mathcal{S}^* = [0, 1]$.

Creating Symmetric Subshapes: The equivalence class of indices is given by $[s^*] = \{-s^*, s^*\}$ which generates subshapes $\tilde{\mathcal{Z}}(\underline{x}, s^*) = \{-s^* \cdot r, s^* \cdot r\}$ that all consist of two opposing sources, as illustrated in Fig. 8(b). As we assumed the occurrence of sources to be uniformly distributed $p(s) = \mathcal{U}[-1, 1]$, the distribution of the subshapes, according to (42), is also uniformly distributed $p(s^*) = \mathcal{U}[0, 1]$.

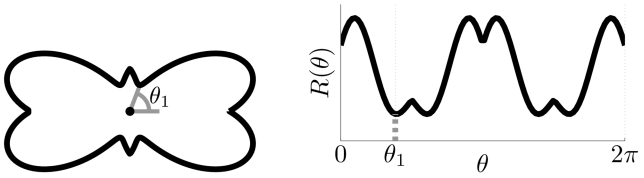

(a) object contour (b) radius function

Fig. 9. The polar function $R(\theta)$ specifies a radius for each angle θ. The correspondence between polar function and shape contour is marked for a given θ_1.

Simplifying the RHM: An appropriate simplified shape function $g^*_{s^*}(\underline{x}, z)$, which only needs to be specified on the positive z-axis and returns 0 for subshapes $\tilde{\mathcal{Z}}(\underline{x}, s^*)$ is given by $g^*_{s^*}(\underline{x}, z) = |z| - s^* \cdot r$. This shape function yields the measurement function

$$\begin{aligned} h(\underline{x}, y, w, s^*) &= g^*_{s^*}(\underline{x}, H(\underline{x}, y - w)) \\ &= |H(\underline{x}, (y - w))| - s^* \cdot r, \end{aligned} \tag{55}$$

which can be immediately used in Alg. 1. It is interesting to compare the measurement functions of the common stick SDM (54) and its simplified version (55). Besides the different integration variables, they only differ in the sense that the simplified SDM additionally requires taking an absolute value. The benefit of using this modified model with a sample-based estimator is that s^* only has to be sampled in $[0, 1]$ instead of $[-1, 1]$. This results in doubling the effective sample resolution.

Extension to Two-Dimensional Space: In two-dimensional space, as seen from the object frame, the stick represents a segment parallel to the z_1-axis that is centered on the origin. Extending the measurement function (54) is straighforward and yields

$$h(\underline{x}, \underline{y}, \underline{w}, s^*) = \begin{bmatrix} g_{s^*}(\underline{x}, (y_1 - w_1)^O) \\ (y_2 - w_2)^O \end{bmatrix} = \begin{bmatrix} 0 \\ 0 \end{bmatrix}, \tag{56}$$

where $[(y_1 - w_1)^O, (y_2 - w_2)^O]^{\mathrm{T}} = H(\underline{x}, \underline{y} - \underline{w})$ represents points transformed into object coordinates using H.

10 Example 2: Star-Convex Object

In [3], an RHM was proposed that models objects with a complex star-convex shape in $\mathbb{R}^2$. Star-convex means that there is a point within the shape, where each line segment to any point on the boundary remains in the shape. This allows for a convenient representation by means of a polar function $R(\theta)$ that gives the radius for a given angle θ from 0 to 2π, as illustrated in Fig. 9. In [3], the radius function $R(\theta)$ is implemented by means of a Fourier series

$$R(\underline{x}, \theta) = \frac{a_0}{2} + \sum_{m=1}^{M} a_m \cos\left(m \frac{2\pi}{P} \theta\right) + b_m \sin\left(m \frac{2\pi}{P} \theta\right). \tag{57}$$

This superposition of cosine and sine functions (with $P = 2\pi$) is weighted by a list of $2M + 1$ coefficients that form the shape vector $\underline{x}^{\text{shape}} = [a_0, a_1, b_1, \ldots, a_M, b_M]^{\mathrm{T}}$. The number of coefficients determines the degree of

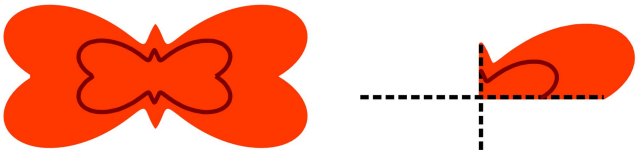

(a) common, $t = 0.5$ (b) proposed, $t = 0.5$

Fig. 10. Difference between modeling a star-convex shape without (a) and with (b) symmetry.

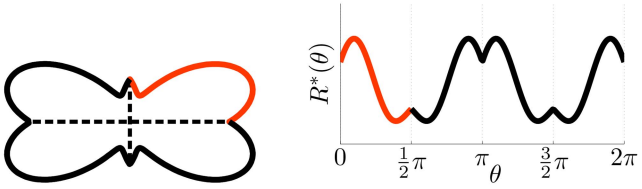

(a) object contour (b) radius function

Fig. 11. Star-convex object with 2-axial symmetry, represented by a polar function. The non-redundant part of the boundary is colored orange.

shape detail the corresponding polar function is capable to encode. For example if $M = 0$, then $R(\underline{x},\theta) = a_0/2$ is independent of θ and specifies the constant radius of a circle.

As we deal with polar functions, in this section, we will occasionally use polar coordinates for points $\underline{z} \in \mathbb{R}^2$, i.e., the radius $r(\underline{z})$, and angle $\theta(\underline{z})$.

10.1 No Symmetry

In [3], a shape $\tilde{\mathcal{Z}}(\underline{x})$ was partitioned into subsets $\tilde{\mathcal{Z}}(\underline{x},t)$, resulting in an RHM according to (17) with shape function

$$g_t(\underline{x},\underline{z}) = r(\underline{z}) - t \cdot R(\underline{x},\theta(\underline{z})). \tag{58}$$

For each parameter $t \in [0,1]$, the shape function determines a set $\tilde{\mathcal{Z}}(\underline{x},t)$ that corresponds to a scaled boundary. Fig. 10(a) shows a visualization for $t = 0.5$ from the shape considered in Fig. 9. When measurement sources are assumed to be uniformly distributed over the object, then it holds that $p(t^2) = \mathcal{U}[0,1]$.

10.2 2-axial Symmetry

For a given shape, let us assume that prior knowledge is available about it having a 2-axial symmetry. We can derive a simplified RHM (38) by specifying an aggregation function and deriving a simplified shape function.

Specifying Aggregation Function: The 2-axial symmetry refers to an aggregation function according to (24) with $n = 2$ that results in the special case $T(\underline{z}) = [|z_1|,|z_2|]^{\mathrm{T}}$, i.e., it maps each point to its symmetric equivalent in the first quadrant. In consequence, the corresponding angles $\theta(\underline{z},n)$ in polar representation lie between 0 and $\pi/2$, as illustrated in Fig. 11.

Simplifying the RHM: Due to the 2-axial symmetry only one fourth of the shape has to be modeled by the radius function (see Fig. 10(b)). In order to take advantage of this reduced domain, we can change the period of the Fourier series from $P = 2\pi$ to $P^* = 2\pi/n$. Then, let $R^*(\underline{x},\theta)$ be a radius function (57) with the adjusted period P^*. The simplified model has the shape function

$$g_t^*(\underline{x},\underline{z}) = r(\underline{z}) - t \cdot R^*(\underline{x},\theta(\underline{z},n)), \tag{59}$$

The corresponding measurement function that incorporates the pose then becomes

$$\begin{aligned} h(\underline{x},\underline{y},\underline{w},t) &= g_t^*(\underline{x},T(H(\underline{x},\underline{y}-\underline{w}))) \\ &= r((\underline{y}-\underline{w})^O) - t \cdot R^*(\theta((\underline{y}-\underline{w})^O,n)) = 0, \end{aligned} \tag{60}$$

which can be immediately used in Alg. 1. The simplification has the benefit that the shape parameters only need to specify the shape in one fourth of the spatial domain, which in turn reduces the complexity of the estimation problem.

REMARK 5 **(Number of Coefficients and Symmetries)** A crucial challenge when designing an estimator based on a symmetric star-convex model is to find the number of coefficients and symmetries which reflect best the geometry of the underlying object. These concepts are not independent from each other, as increasing the number of symmetries yields a higher shape detail while maintaining the same number of coefficients. As such, even when an object is not perfectly symmetric, assuming symmetry anyway can yield an improved shape estimate. However, then the estimator finds parameters of an intermediate symmetric shape and loses the ability of a perfect shape estimate. In order to explore this trade-off, the evaluation in Sec. 11.2 includes an extensive analysis related to varying number of coefficients and symmetries.

As another short remark, note that it would also have been possible to enforce symmetry by constraining the coefficients of the Fourier series. However, these considerations would be out of the scope of this work, as our intention is to demonstrate the universality of the proposed simplification approach.

11 EVALUATION

In this section, we evaluate the proposed approach by means of a simulated tracking scenario. Our intention is to investigate the effect of applying symmetric simplification to the common models from the previous examples. As such, we exclusively focus in this work on comparing estimators based on a common non symmetric model with its symmetric version. As an example, we chose tracking the symmetric airplane object from the motivating example in Fig. 1 while following the

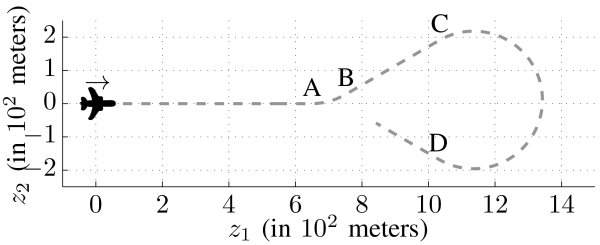

Fig. 12. Evaluation Scenario: plane object moves along the dashed, gray path with constant speed. This path is composed of three straight, and two circular parts. The labels A–D mark changes between the different motion parts.

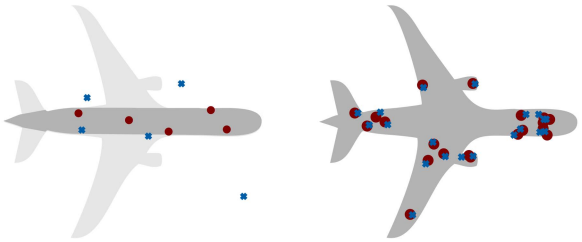

(a) low information scenario (b) high information scenario

Fig. 13. Few measurements from fuselage with high noise for the stick evaluation (a). Many measurements from entire plane with low noise for the star-convex evaluation (b). Measurement sources are marked by red circles, measurements by blue crosses.

path depicted in Fig. 12. The object moves with constant speed and is observed by a simulated sensor. The evaluation is divided into two parts, consisting of a *low information* scenario using a stick model (Sec. 9), and a *high information* scenario using a star-convex model (Sec. 10). In the following, we differentiate between the *common approach* without using any symmetry and the *proposed approach*, which incorporates the given symmetries.

Sensor: For the low information scenario using the stick model, we implemented a sensor that obtains one to five measurements each time step uniformly from the fuselage of the airplane. The number n_k of measurements is uniformly drawn from $\{1,\dots,5\}$. The fuselage has a size of 100 m length and 20 m meters width, and its measurement sources are uniformly distributed on its extent. During observation, these measurements are corrupted with high noise, modeled as zero-mean Gaussian noise according to $\mathcal{N}(\underline{0}, 10^2 \cdot \mathbf{I})$.

For the high information scenario based on the more detailed star-convex model, the sensor obtains ten to twenty measurements each time step uniformly from the entire plane, which has a size of 100 m length and 90 m width. Again, the number n_k of measurements is uniformly drawn from $\{1,\dots,20\}$. Then, these measurements are disturbed using zero-mean Gaussian noise according to $\mathcal{N}(\underline{0}, 10^0 \cdot \mathbf{I})$. Example measurements from both sensors are illustrated in Fig. 13.

Pose and Motion: In order to reflect the authentic behavior of a plane, the path in Fig. 12 was chosen to switch between straight and circular movements. The speed was chosen to be about 50 m per time step so that it takes 400 time steps to complete one run. At each time step k, the pose model uses a rigid transformation where the parameters to be estimated are $\underline{x}_k^{\text{pose}} = [\phi_k, \underline{t}_k^{\mathrm{T}}]^{\mathrm{T}}$, with ϕ_k as the orientation angle, and $\underline{t}_k \in \mathbb{R}^2$ as the translation vector.

In addition, we use a motion model that assumes a constant speed and a constant turn rate, similar to [21]. This model requires estimating two further state parameters, $\underline{x}_k^{\text{motion}} = [\dot{\phi}_k, v_k]^{\mathrm{T}}$, where $\dot{\phi}_k$ is the angular speed, and v_k is the object speed. The velocity is then assumed to be the vector $[1,0]^T$ rotated by the orientation ϕ_k and scaled by the magnitude v_k. We do not employ any switching structure.

TABLE I
Compared approaches in the stick tracking experiment.

	UKF [10]	S^2KF [23]
no symmetry (quad. extension) [1]	common-1	common-2
1-axial symmetry	proposed-1	proposed-2

11.1 Tracking Stick Object

First, we look at the low information scenario with the stick model. We compare the common approach from [1] to the modified approach that exploits the 1-axial symmetry, both explained in Sec. 9. Both models require estimating the shape parameter $\underline{x}_k^{\text{shape}} = r_k$. The combined state parameters form the 6×1 vector $\underline{x}_k = [(\underline{x}_k^{\text{pose}})^{\mathrm{T}}, (\underline{x}_k^{\text{shape}})^{\mathrm{T}}, (\underline{x}_k^{\text{motion}})^{\mathrm{T}}]^{\mathrm{T}}$. From the initial measurements, where we required a minimum of two points, $\underline{x}_0^{\text{pose}}$ was determined by total least squares, r_k from $\underline{x}_0^{\text{shape}}$ was set to half of the distance between the farthest points, and $\underline{x}_0^{\text{motion}}$ was initialized to $\underline{0}$. The initial state covariance matrix was set to $\mathbf{C}_{\underline{x}_0} = \text{diag}(10^{-2}, 10^3, 10^3, 10, 10^{-3}, 10)$. The system covariance matrix was set to the constant $\text{diag}(10^{-9}, 10^{-7}, 10^{-7}, 1, 10^{-6}, 10^{-3})$. Then, 100 runs of the experiment were performed.

We compare two sample-based estimators, both based on the common model and the proposed model, as depicted in Tab. I. The UKF was implemented according to [10], using two samples per dimension plus one, and parameters $\alpha = 1$, $\beta = 0$, $\kappa = 1/2$. The S^2KF was implemented according to [23] using five samples per dimension.

Results: The *root mean squared errors* (RMSEs) for position, angle and stick length are depicted in Fig. 15. In the estimated pose parameters, all approaches show a quite similar performance, i.e., about 4 m position error and 3° orientation error. Note that all estimators need some time steps to adapt to the motion changes at A, B, C, and D, as we do not use any switching motion models. As an important result, it can be seen that "proposed-1" and "proposed-2" both perform better in estimating the length of the stick. As can be seen in Fig. 15(c), the common SDM [1] imposes special

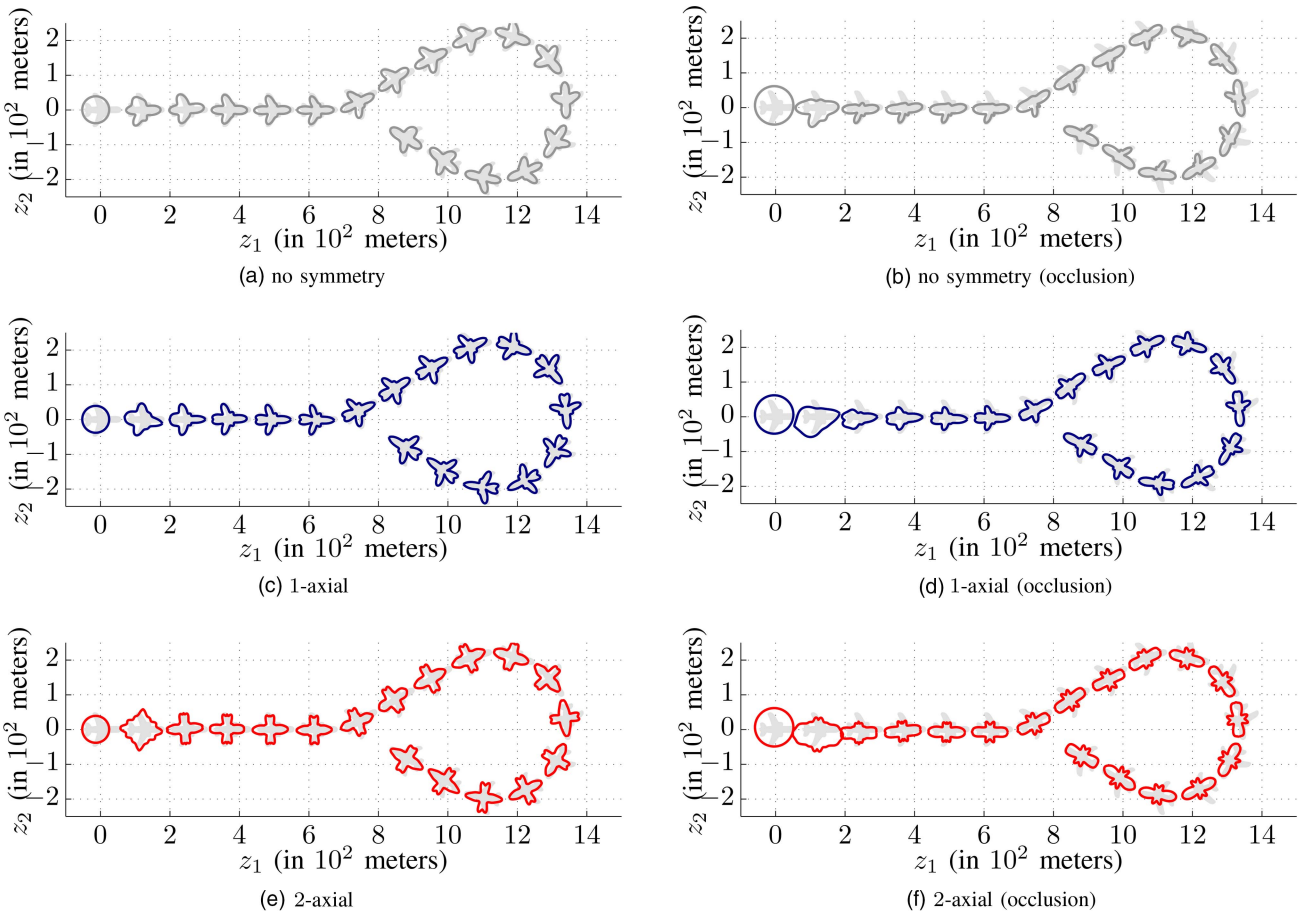

(a) no symmetry (b) no symmetry (occlusion)

(c) 1-axial (d) 1-axial (occlusion)

(e) 2-axial (f) 2-axial (occlusion)

Fig. 14. Estimation result of the star-convex shape when using 13 Fourier coefficients for selected time steps.

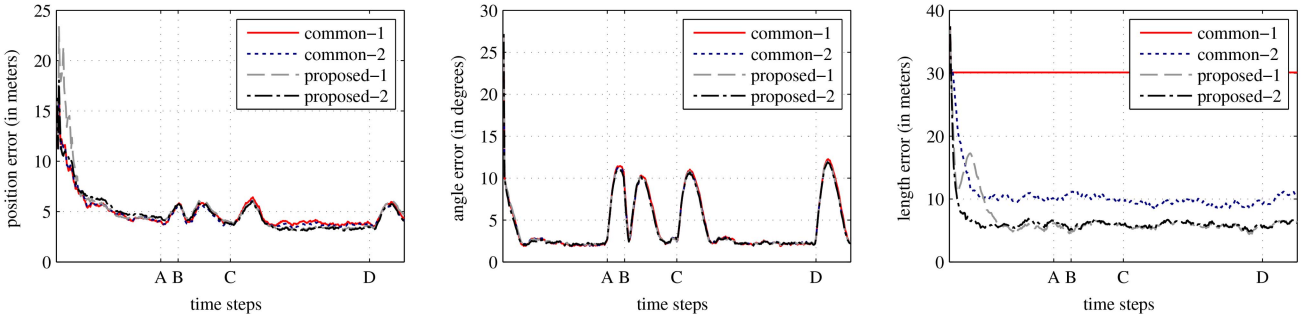

(a) position RMSE (b) angle RMSE (c) length RMSE

Fig. 15. Evaluation of the stick object.

requirements to the filter being used, as "common-2" estimates the length correctly and "common-1" does not. In contrast, the simplified SDM in "proposed-1" and "proposed-2" has no special requirements to the filter being used. This is a significant improvement, especially because the simple UKF in "proposed-1" also outperforms the advanced S^2KF in "common-2."

11.2 Tracking Star-convex Object

Next, we performed the high information experiment using the star-convex models presented in Sec. 10. We compare the common RHM-approach from [3] to the modified approach based on a simplified RHM that assumes different axial symmetries. In addition, we varied the amount of Fourier coefficients in order to investigate their effects on the estimation result. Specifically, we set up models with "no symmetry," "1-axial symmetry," and "2-axial symmetry," each with $M = 3, 5, 7, 9, 11, 13$, and 15 coefficients, respectively.

A UKF [10] with equal parametrization as in the previous scenario was used for estimating the parameters of all models. The combined state parameters form the $(5 + M) \times 1$ vector $\underline{x}_k = [(\underline{x}_k^{\text{pose}})^{\text{T}}, (\underline{x}_k^{\text{shape}})^{\text{T}}, (\underline{x}_k^{\text{motion}})^{\text{T}}]^{\text{T}}$. From the initial measurements, where we required a mini-

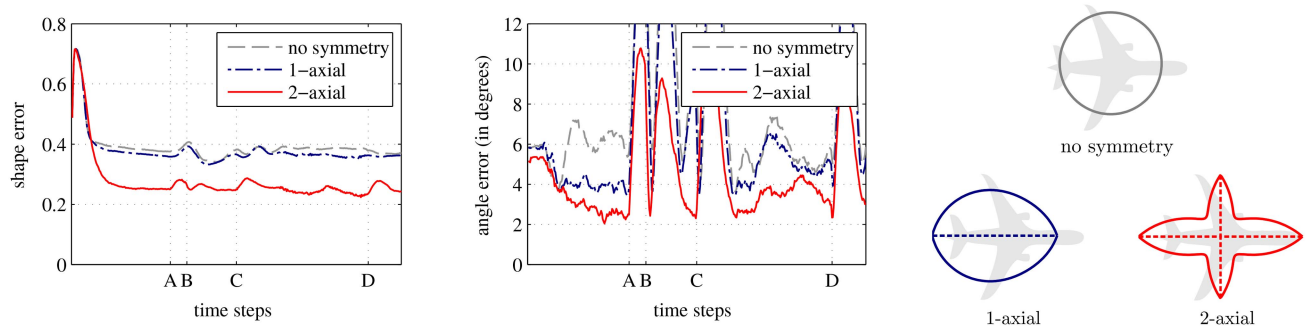

(a) shape RMSE (b) angle RMSE (c) representative estimated shape

Fig. 16. Evaluation of the star-convex object with 3 Fourier coefficients.

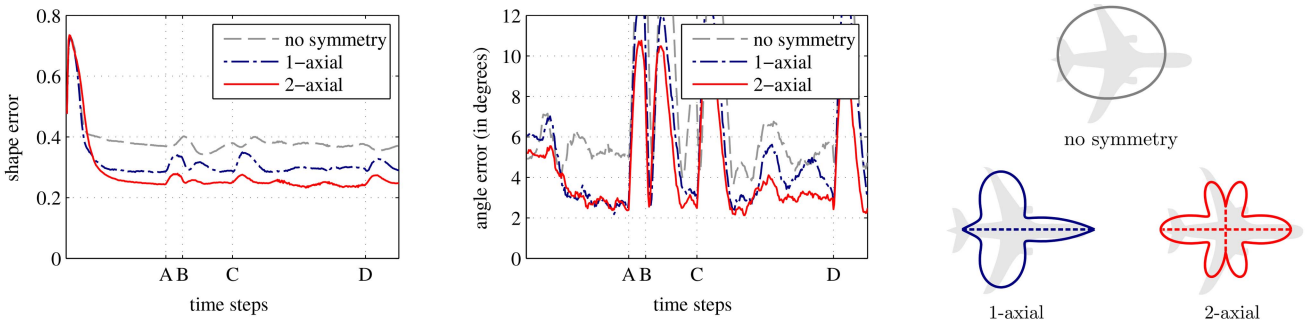

(a) shape RMSE (b) angle RMSE (c) representative estimated shape

Fig. 17. Evaluation of the star-convex object with 5 Fourier coefficients.

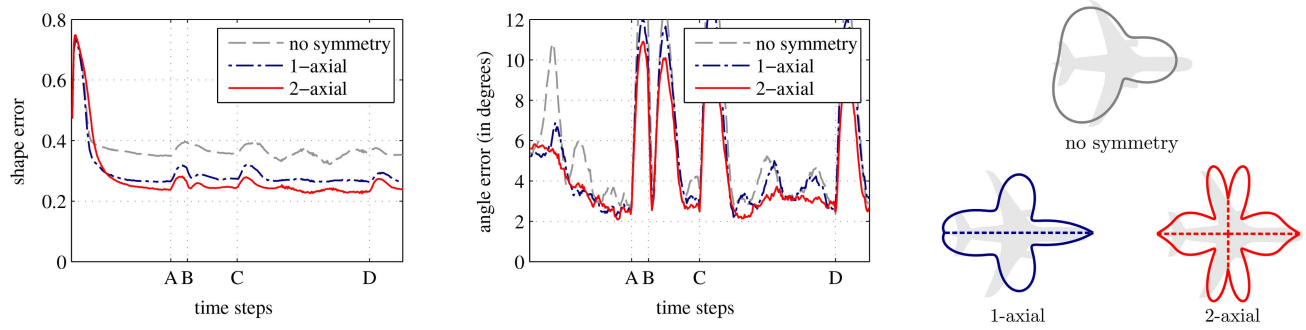

(a) shape RMSE (b) angle RMSE (c) representative estimated shape

Fig. 18. Evaluation of the star-convex object with 7 Fourier coefficients.

mum of two points, $\underline{x}_0^{\text{pose}}$ was determined as follows. The mean of the points was used as $\underline{t}_0$, and the orientation was set to $\theta_k = 0$. For $\underline{x}_0^{\text{shape}}$, the first Fourier coefficient was set to half of the distance between the farthest points, and all others to zero, which corresponds to a circle with mean $\underline{t}_0$ and radius given by the first coefficient. Again $\underline{x}_0^{\text{motion}}$ was initialized with $\underline{0}$. The initial state covariance was set to $\mathbf{C}_{\underline{x}_0} = \text{diag}(10^{-1}, 10^{3}, 10^{3}, 10^{-1}, \ldots, 10^{-3}, 10)$. The system covariance matrix was set to the constant $\text{diag}(10^{-6}, 10^{-2}, 10^{-2}, 10^{-6}, \ldots, 10^{-6}, 10^{-2})$. Then, 100 runs of the experiment were performed.

Results: In order to compare estimation results of the different approaches we chose the "intersection over union" [5], where we calculated an RMSE from $1 - (\textit{intersection}/\textit{union})$. Its values range from 1 to 0, where 0 means no intersection of the estimate and the groundtruth and 0 means a perfect match. The behavior of this error, as shown Fig. 16–22(a), indicates the convergence behavior of the shape, as well as the position. The estimation process over a run is illustrated in Fig. 14(a,c,e). Representative shape estimates after a single run are depicted in Fig. 16–22(c), respectively. In addition, Fig. 16–22(b) shows the RMSE of the estimated heading angle. All approaches initially converge no later than time step A and, particularly, we did not observe any run, where the estimator diverged. The increased error at time steps A, B, C, D, are caused by the changing motion of the plane.

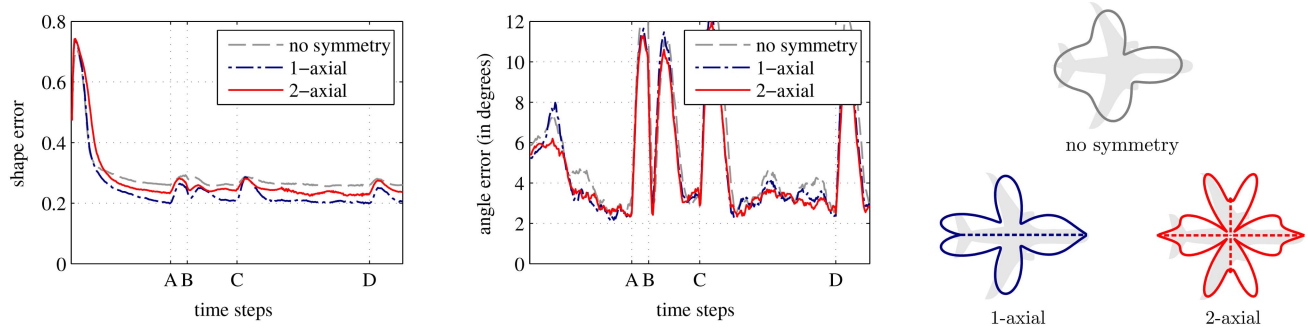

(a) shape RMSE (b) angle RMSE (c) representative estimated shape

Fig. 19. Evaluation of the star-convex object with 9 Fourier coefficients.

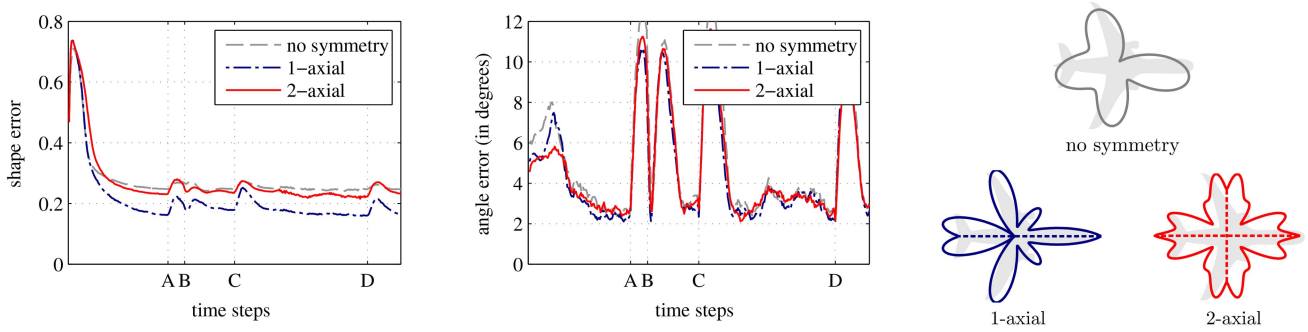

(a) shape RMSE (b) angle RMSE (c) representative estimated shape

Fig. 20. Evaluation of the star-convex object with 11 Fourier coefficients.

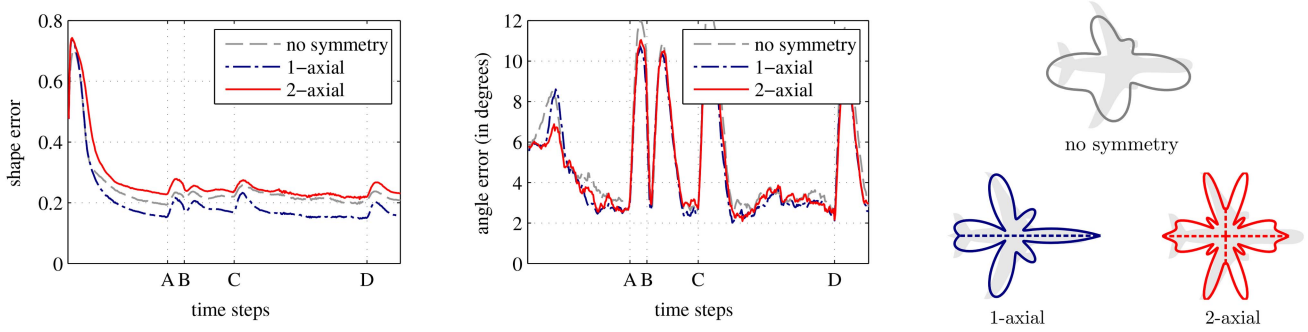

(a) shape RMSE (b) angle RMSE (c) representative estimated shape

Fig. 21. Evaluation of the star-convex object with 13 Fourier coefficients.

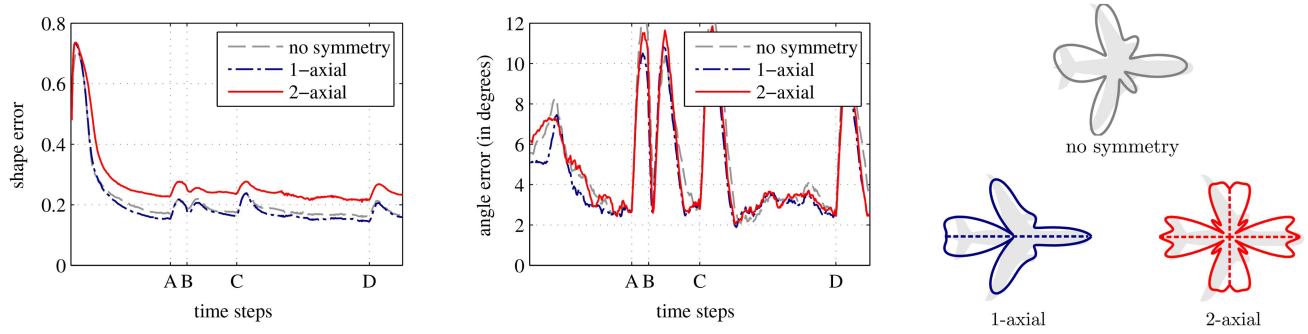

(a) shape RMSE (b) angle RMSE (c) representative estimated shape

Fig. 22. Evaluation of the star-convex object with 15 Fourier coefficients.

Let us now discuss the trade-off between number of coefficients and symmetries, as mentioned in Remark 5. The proposed approach with 1-axial symmetry outperforms the common approach for all numbers of coefficients. Introducing the second symmetry axis yields a benefit over the 1-axial approach up to seven coefficients as the additional symmetry results in the capability of capturing a higher degree of shape detail while maintaining the number of parameters. This can particularly be seen in Fig. 16(c), where the 2-axial finds a reasonable shape when using only three Fourier coefficients. The 1-axial model (and the common approach) are not capable of representing the shape before five (seven respectively) parameters are introduced.

However, for the case when a higher number of Fourier coefficients is used, the 1-axial model steadily outperforms the 2-axial model, as the underlying shape, i.e., the plane, has only a 1-axial symmetry. Note that the 2-axial approach is never capable of estimating the shape correctly, as it always converges to an intermediate shape. For the common approach, it is worth pointing out that the estimated result never displays any of the underlying symmetries. Again, it should be noted that, as with the stick, incorporating symmetry into the star-convex model yields a superior tracking result while only marginally changing the generative model.

Results Under Partial Occlusion: In order to evaluate the effect of using symmetries in the presence of occlusion, we modified the high information scenario by removing all measurements from the left wings of the plane. Qualitative results are shown in Fig. 14(b,d,f). As expected, the common approach estimates a non-symmetric shape without the left wings. In contrast, the proposed approaches impose symmetric constraints and, thus, estimate shapes which have wings on both sides. It is remarkable that the symmetry axes are found, even though there are no measurements from the left side at any time. This is due to the fact that the model assumes symmetry with respect to the direction of velocity.

12 CONCLUSION

In this work, we presented a concept for designing a simplified Bayesian estimator for extended object tracking that exploits symmetries in the object geometry. We proposed simplification of estimators based on Spatial Distribution Models (SDM), Greedy Association Models (GAM), and Random Hypersurface Models (RHM). The key idea is to aggregate equivalent points according to the object symmetry, such that the source model only needs to be evaluated in the non-redundant part of the spatial domain. In doing so, a simplification scheme was obtained that yields two major improvements:

1. For all source models, simplified versions can be derived that allow for reducing the number of shape parameters while estimating an equally detailed shape. The benefit to expect is proportional to the reduction of the spatial extent from the entire shape to the non-redundant part.
2. Simplifying SDMs additionally requires aggregating symmetric sources and their individual probabilities. This aggregation turns the SDM into an RHM that achieves a higher spatial sample resolution in sample-based filters. The benefit is again in the same order of magnitude, as it also depends on the ratio between the spatial extent of the entire shape and its non-redundant part.

Both simplifications reduce the complexity of the estimation problem and yield an improved estimation result, as we illustrated by means of two examples: A simple stick object and a star-convex object. In particular, we showed that applying the proposed simplification to a common stick model yields an RHM that can be used with a UKF, while the original model requires a more advanced filter. In numerical terms, the proposed new stick RHM reduces the length error about 60%. Using the symmetric star-convex model in the considered scenario reduces the orientation error up to 50%, and the shape error up to 30%, depending on the number of Fourier coefficients. As an additional benefit, we showed that our approach uses measurement information from visible parts of the object in order to infer the shape of occluded, symmetric counterparts.

Future research will include a closer look at the effect that object symmetries have in the estimated state density, particularly in the form of multiple modes. Incorporating a mechanism that automatically chooses the appropriate type of symmetry, e.g., based on a symmetric descriptor [11], is also an interesting research topic. Finally, it is also worth exploring and evaluating other types of symmetry, e.g., periodicity, in order to simplify source models for a wider spectrum of shapes.

REFERENCES

[1] M. Baum, F. Faion, and U. D. Hanebeck
Modeling the Target Extent with Multiplicative Noise.
In *Proceedings of the 15th International Conference on Information Fusion (FUSION)*, pages 2406–2412, Singapore, 2012.

[2] M. Baum and U. D. Hanebeck
Random Hypersurface Models for Extended Object Tracking.
In *2009 IEEE International Symposium on Signal Processing and Information Technology (ISSPIT)*, pages 178–183, Ajman, United Arab Emirates, Dec. 2009. IEEE.

[3] M. Baum and U. D. Hanebeck
Shape Tracking of Extended Objects and Group Targets with Star-Convex RHMs.
In *Proceedings of the 14th International Conference on Information Fusion (FUSION)*, pages 1–8, Chicago, Illinois, USA, 2011.

[4] M. Baum, V. Klumpp, and U. D. Hanebeck
A Novel Bayesian Method for Fitting a Circle to Noisy Points.
In *Proceedings of the 13th International Conference on Information Fusion (FUSION)*, Edinburgh, United Kingdom, 2010.

[5] Benjamin Sapp, Chris Jordan, and Ben Taskar
Adaptive Pose Priors for Pictorial Structures.
In *IEEE Conference on Computer Vision and Pattern Recognition (CVPR)*, pages 422–429, San Francisco, USA, 2010.

[6] F. Faion, M. Baum, and U. D. Hanebeck
Tracking 3D Shapes in Noisy Point Clouds with Random Hypersurface Models.
In *Proceedings of the 15th International Conference on Information Fusion (FUSION)*, pages 2230–2235, Singapore, 2012.

[7] F. Faion, A. Zea, and U. D. Hanebeck
Reducing Bias in Bayesian Shape Estimation.
In *IEEE 17th International Conference on Information Fusion (FUSION)*, pages 1–8, Salamanca, Spain, 2014. IEEE.

[8] M. Feldmann, D. Franken, and W. Koch
Tracking of Extended Objects and Group Targets Using Random Matrices.
IEEE Transactions on Signal Processing, 59(4):1409–1420, Apr. 2011.

[9] K. Gilholm and D. Salmond
Spatial Distribution Model for Tracking Extended Objects.
IEE Proceedings on Radar, Sonar and Navigation, 152(5): 364–371, 2005.

[10] S. J. Julier and J. K. Uhlmann
Unscented Filtering and Nonlinear Estimation.
Proceedings of the IEEE, 92(3):401–422, Mar. 2004.

[11] M. Kazhdan, T. Funkhouser, and S. Rusinkiewicz
Symmetry Descriptors and 3D Shape Matching.
In *Proceedings of the 2004 Eurographics/ACM SIGGRAPH symposium on Geometry processing—SGP*, pages 115–123, New York, New York, USA, 2004. ACM Press.

[12] G. Kurz, I. Gilitschenski, S. J. Julier, and U. D. Hanebeck
Recursive Estimation of Orientation Based on the Bingham Distribution.
In *Proceedings of the 16th International Conference on Information Fusion (FUSION)*, pages 1487–1494, Istanbul, Turkey, 2013.

[13] J. Lan and X. R. Li
Tracking of Maneuvering Non-Ellipsoidal Extended Object or Target Group Using Random Matrix.
IEEE Transactions on Signal Processing, 62(9):2450–2463, May 2014.

[14] W. F. Leven and A. D. Lanterman
Unscented Kalman Filters for Multiple Target Tracking With Symmetric Measurement Equations.
IEEE Transactions on Automatic Control, 54(2):370–375, Feb. 2009.

[15] W. Li and L. Kleeman
Real Time Object Tracking Using Reflectional Symmetry and Motion.
In *International Conference on Intelligent Robots and Systems (IROS)*, pages 2798–2803, Beijing, China, 2006.

[16] S. Loncaric
A Survey of Shape Analysis Techniques.
Pattern Recognition, 31:983–1001, 1998.

[17] N. J. Mitra, M. Pauly, M. Wand, and D. Ceylan
Symmetry in 3D Geometry: Extraction and Applications.
Computer Graphics Forum, 32(6), 2013.

[18] N. Petrov and L. Mihaylova
A Novel Sequential Monte Carlo Approach for Extended Object Tracking Based on Border Parameterisation.
In *Proceedings of the 14th International Conference on Information Fusion (FUSION)*, pages 306–313, Chicago, Illinois, USA, 2011.

[19] T. Riklin-Raviv, N. Kiryati, and N. Sochen
Segmentation by Level Sets and Symmetry.
In *IEEE Computer Society Conference on Computer Vision and Pattern Recognition (CVPR)*, volume 1, pages 1015–1022, New York, NY, USA, 2006.

[20] A. Rivers, F. Durand, and T. Igarashi
3D Modeling with Silhouettes.
ACM Transactions on Graphics, 29(4):1, July 2010.

[21] X. Rong Li and V. Jilkov
Survey of Maneuvering Target Tracking. Part I: Dynamic Models.
IEEE Transactions on Aerospace and Electronic Systems, 39(4):1333–1364, Oct. 2003.

[22] P. Simari, E. Kalogerakis, and K. Singh
Folding Meshes: Hierarchical Mesh Segmentation Based on Planar Symmetry.
In *Eurographics Symposium on Geometry Processing*, 2006.

[23] J. Steinbring and U. D. Hanebeck
S2KF: The Smart Sampling Kalman Filter.
In *Proceedings of the 16th International Conference on Information Fusion (FUSION)*, pages 2089–2096, Istanbul, Turkey, 2013.

[24] M. Werman and D. Keren
A Bayesian Method for Fitting Parametric and Nonparametric Models to Noisy Data.
IEEE Transactions on Pattern Analysis and Machine Intelligence, 23(5):528–534, 2001.

Florian Faion received his Dipl.-Inform. in computer science from the Karlsruhe Institute of Technology (KIT), Germany, in 2010. Currently, he is working towards a Ph.D. degree at the Intelligent Sensor-Actuator-Systems Laboratory, Karlsruhe Institute of Technology (KIT), Germany. His research interests are in the field of extended object tracking, shape estimation and telepresence.

Antonio Zea received his Dipl.-Inform. in computer science from the Karlsruhe Institute of Technology (KIT), Germany, in 2013. Currently, he is working towards a Ph.D. degree at the Intelligent Sensor-Actuator-Systems Laboratory, Karlsruhe Institute of Technology (KIT), Germany. His research interests are in the field of extended object tracking, shape estimation and telepresence.

Marcus Baum is an assistant research professor at the University of Connecticut. He received his Dipl.-Inform. degree in computer science from the Universitaet Karlsruhe (TH), Germany, in 2007, and his a Dr.-Ing. degree at the Intelligent Sensor-Actuator-Systems Laboratory, Karlsruhe Institute of Technology (KIT), Germany, in 2013. His research interests are in the field of extended object tracking, nonlinear estimation, and sensor data fusion. Since 2014, he is the associate administrative editor for the Journal of Advances in Information Fusion (JAIF).

Uwe D. Hanebeck is a chaired professor of Computer Science at the Karlsruhe Institute of Technology (KIT) in Germany and director of the Intelligent Sensor-Actuator-Systems Laboratory (ISAS). Since 2005, he is the chairman of the Research Training Group RTG 1194 "Self-Organizing Sensor-Actuator-Networks" financed by the German Research Foundation.

Prof. Hanebeck obtained his Ph.D. degree in 1997 and his habilitation degree in 2003, both in Electrical Engineering from the Technical University in Munich, Germany.

His research interests are in the areas of information fusion, nonlinear state estimation, stochastic modeling, system identification, and control with a strong emphasis on theory-driven approaches based on stochastic system theory and uncertainty models. Research results are applied to various application topics like localization, human-robot-interaction, assistive systems, sensor-actuator-networks, medical engineering, distributed measuring system, and extended range telepresence. Research is pursued in many academic projects and in a variety of cooperations with industrial partners.

Uwe D. Hanebeck was the General Chair of the "2006 IEEE International Conference on Multisensor Fusion and Integration for Intelligent Systems (MFI 2006)," Program Co-Chair of the "11th International Conference on Information Fusion (Fusion 2008)," Program Co-Chair of the "2008 IEEE International Conference on Multisensor Fusion and Integration for Intelligent Systems (MFI 2008)," Regional Program Co-Chair for Europe for the "2010 IEEE/RSJ International Conference on Intelligent Robots and Systems (IROS 2010)," and will be General Chair of the "19th International Conference on Information Fusion (Fusion 2016)." He is a Member of the Board of Directors of the International Society of Information Fusion (ISIF), Editor-in-chief of its Journal of Advances in Information Fusion (JAIF), and associate editor for the letter category of the IEEE Transactions on Aerospace and Electronic Systems (TAES). He is author and coauthor of more than 350 publications in various high-ranking journals and conferences.